***Military Technical College***
***Kobry El-Kobbah,***
***Cairo, Egypt.***

***16th International Conference on Applied Mechanics and Mechanical Engineering.***

# MODELING AND ANALYSIS OF SHAPE MEMORY ALLOY LAMINATED COMPOSITE PLATES

M. K. Abbas*, M. A. Elshafei* and H. M. Negm†

## ABSTRACT

In the present work, laminated composite plates with surface bonded shape memory alloy sheets are modeled and analyzed based on the modified higher-order shear deformation theory. The energy balance equations in conjunction with Brinson's SMA constitutive model are used to formulate the heat transfer governing equations. The static responses as well as dynamic characteristics of the plates are obtained using Ritz solution technique. The plates are subjected to mechanical loads with two types of boundary conditions, simply-supported and cantilevered. A Mathematica code is developed to analyze different plate problems. The time response of the shape memory alloy laminated composite plate is studied. The obtained results are compared to the available studies solved by different theories. Parametric studies are conducted to demonstrate the effect of thickness ratio, aspect ratio, material properties, thermal expansion coefficient, and thickness of shape memory alloy sheet on the transverse deflections, natural frequencies, and response time.

## KEY WORDS

Shape memory alloys, composite plate, Higher-order shear deformation theory, heat transfer modeling, Ritz energy method, static and dynamic analysis of plates.

---

* Egyptian Armed Forces.
† Department of Aerospace Engineering, Cairo University, Cairo, Egypt.

## NOMENCLATURE

| | |
|---|---|
| $\alpha$ | Thermal expansion coefficient of the SMA material |
| $\{\gamma\}$ | The unknown displacements vector |
| $\{\varepsilon\}$ | Strain vector in x-y-z coordinates |
| $\{\sigma\}$ | Stress vector in x-y-z coordinates |
| $\left[\bar{Q}\right]_i$ | Transformed stiffness matrix of layer (i) |
| $\delta U$ | Virtual strain energy |
| $\delta V$ | Virtual work |
| $\delta K$ | Virtual kinetic energy |
| $\{a(x,y)\}$ | Column vectors of the Ritz approximation functions that satisfy the boundary conditions of the problem |
| $\{q(t)\}$ | Column vectors of the Ritz coefficients |
| $[K]$ | Stiffness matrix |
| $[M]$ | Mass matrix |
| $p_z, F_{zi}$ | Distributed and concentrated loads |
| $\{F\}, \{F_0\}$ | Distributed and concentrated load vectors |
| A | Plate's area |
| a, b | Plate sides' dimensions |
| A, B, D | Extensional, coupling, and bending stiffness matrices |
| E, F, H, J | Higher order stiffness matrices |
| h | Total laminate thickness |
| $I_i$ | Inertia terms |
| k | Total number of layers |
| q | transverse uniform load |
| u | Displacement of a generic point in the plate in the x direction |
| $u_0$ | Displacement of the geometric mid-plane in the x direction |
| v | Displacement of a generic point in the plate in the y direction |
| V | Plate's volume |
| $v_0$ | Displacement of the geometric mid-plane in the y direction |
| w | Displacement of a generic point in the plate in the z direction |
| $w_0$ | Displacement of the geometric mid-plane in the z direction |
| $\theta_x$ | Rotation of the normal to the mid-plane about the y-axis |
| $\theta_y$ | Rotation of the normal to the mid-plane about the x-axis |
| $\theta_z$ | First order displacement factor |
| $\xi_x, \xi_y$ | Third order displacements or warping functions |
| $\psi_x, \psi_y, \psi_z$ | Second order displacements or warping functions |

## INTRODUCTION

The SMA has been a subject of intensive researches in the last decades due to its unique properties of one and two way shape memory effect (SME), pseudo elasticity and high damping capacity.

Ghomshei et. al [1, 2], proposed a nonlinear finite element model and experimental test for the time response of a shape memory alloy (SMA) actuator composed of

matrix material with SMA sheets or wires embedded in or bonded to the matrix part. The model is developed based on a higher order shear deformation beam theory together with the von- Karman strain field. A one-dimensional constitutive equation with non- constant material functions and sinusoidal phase transformation kinetics is used to model the thermo-mechanical behavior of the SMA actuator. The constitutive and phase transformation kinetic equations make distinction between the stress-induced and temperature-induced martensite fraction.

Balapgol et. al [3, 4], studied the deflection, natural frequency and time response of shape memory alloy laminated composite plate using finite element model with first order shear deformation theory. The composite plate consists of a thin layer of SMA bonded to elastomer core. They concluded that the input power, heat sink strength, thermal conductivity, and thickness of the elastomer layer play important roles for controlling the time response of the SMA laminated actuator.

Gordaninejad et. al [5], presented a two dimensional finite element model based on classical lamination theory, energy balance equations, and two-dimensional transition model of SMA layer for the response of thermally driven SMA/ elastomer actuator. Wu et. al [6], derived a closed form solutions for the stress-strain-temperature response of a thermally driven shape memory alloy composite actuator neglecting the heat conduction in axial direction.

Rogers et. al [7] used the Rayleigh-Ritz method to perform a linear analysis for simply-supported plate embedded with SMA fibers. They studied the plate deflection, free vibration, buckling, and acoustic control.

Lin et. al [8] proposed a closed form solution for symmetric composite beams embedded with SMA fibers with various boundary conditions. The resultant actuation forces and normal stress distribution were calculated for the proposed beams.

One of the earliest models is the one-dimensional Tanaka's [9], a macroscopic model that is derived from thermodynamic concepts and through experimental observations. Martensitic transformation was considered progressive through an internal variable, the volume fraction of martensite, ξ. The evolutionary equation was determined by considering the transformation micro-mechanism and it is expressed using an exponential function in the form of $\xi = \xi(\sigma, T)$

Liang and Rogers [10], improved Tanaka's model by directly matching experimental results to get the evolutionary equation which is expressed using the cosine function. The constitutive equation remains the same while the equations' parameters are determined through experiments.

An improvement of the Tanaka's model was made by Brinson [11, 12], who recognized that not all martensite that are converted to austenite will produce the recovery stress. Only the stress induced martensite that is responsible for the shape memory effect. The martensite fraction is divided into two components: stress induced and temperature induced martensite. This model also does not assume constant material functions in the constitutive relationship. Furthermore, Brinson made some amendment that the constitutive equation will be valid at any

temperature. This model was found to give a better representation of the SMA behaviors than the Liang and Rogers's model [10].

In the present study the transverse deflection, natural frequency, and time response of laminated composite plates with surface bonded shape memory alloy sheets are investigated. The analytical model is deduced based on the modified higher-order shear deformation theory utilizing Ritz solution technique. The energy balance equations in conjunction with Brinson's SMA constitutive model are used to formulate the heat transfer equations. Two types of boundary conditions are studied, simply-supported and cantilevered. A Mathematical code is developed to analyze different plates and to validate the obtained results. Parametric studies are performed to demonstrate the effect of the plate thickness ratio, aspect ratio, thermal expansion coefficient, and shape memory alloy sheet thickness on the plate transverse deflections, natural frequencies, and shape memory alloy response time.

## DISPLACEMENT FIELD EQUATIONS

The layout of a shape memory alloy composite plate actuator is shown in Figure 1. The plate consists of a layer of SMA of thickness $t_s$, which is bonded to a composite plate of thickness $(h - t_s)$. The plate length and width are $a$, and $b$, respectively. The plate is bonded at its bottom to a heat sink maintained at temperature $T_{\text{sink}}$. The plate is subjected to a uniform transverse load, $q$. The Cartesian coordinate system is taken so that the $xy$-plane coincides with the mid-plane of the plate, and the z-axis is upward normal to the mid-plane. The displacement field equations of the modified higher order plate theory (MHPT), [13, 14], are given as:

$$\begin{aligned} u(x,y,z,t) &= u_0 + z\left(\theta_x - \frac{\partial w_0}{\partial x}\right) + z^2\psi_x + z^3\xi_x \\ v(x,y,z,t) &= v_0 + z\left(\theta_y - \frac{\partial w_0}{\partial y}\right) + z^2\psi_y + z^3\xi_y \\ w(x,y,z,t) &= w_0 + z\theta_z + z^2\psi_z \end{aligned} \tag{1}$$

The basic assumptions are that the SMA layer and the host layers are perfectly bonded, both thermal stresses and temperature in the phase transformation of SMA are considered, and the plate undergoes a small displacement.

## STRAIN-DISPLACEMENT RELATIONSHIPS

The strain-displacement relationships can be expressed in a matrix form as follows, [13, 14]:

$$\{\varepsilon\} = \{\varepsilon^0\} + z\{\varepsilon^1\} + z^2\{\varepsilon^2\} + z^3\{\varepsilon^3\} \tag{2}$$

where

$$\{\varepsilon\}^T = \begin{bmatrix} \varepsilon_{xx} & \varepsilon_{yy} & \varepsilon_{zz} & \gamma_{yz} & \gamma_{zx} & \gamma_{xy} \end{bmatrix} \tag{3}$$

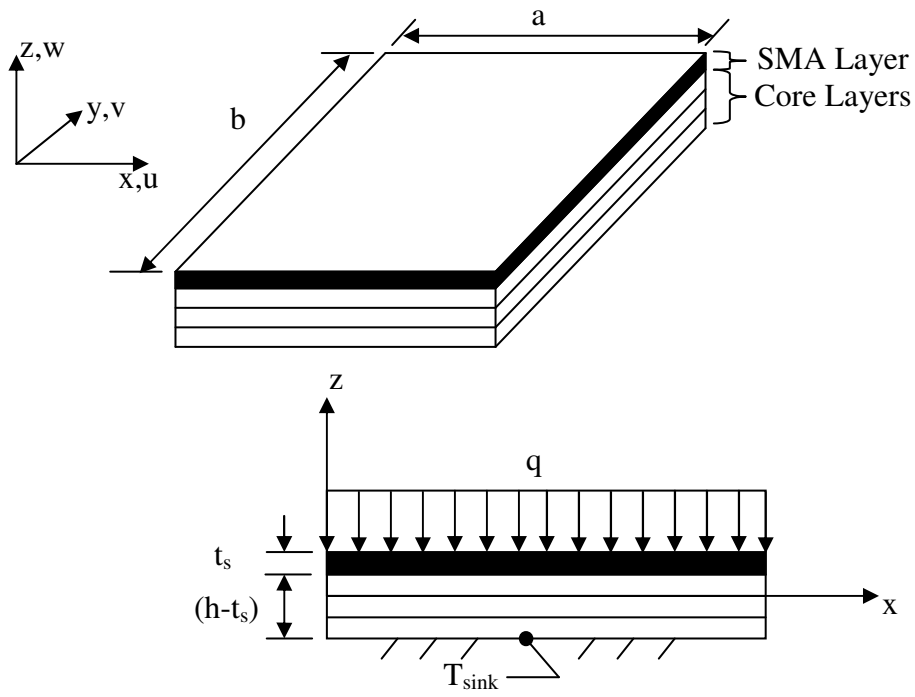


**Figure 1.** SMA laminated plate with applied loading.

and

$$\left\{\varepsilon^0\right\}^T=\left[\frac{\partial u_0}{\partial x}\quad\frac{\partial v_0}{\partial y}\quad\theta_z\quad\theta_y\quad\theta_x\quad\frac{\partial u_0}{\partial y}+\frac{\partial v_0}{\partial x}\right]$$

$$\left\{\varepsilon^1\right\}^T=\left[\frac{\partial\theta_x}{\partial x}-\frac{\partial^2 w_0}{\partial x^2}\quad\frac{\partial\theta_y}{\partial y}-\frac{\partial^2 w_0}{\partial y^2}\quad 2\psi_z\quad 2\psi_y+\frac{\partial\theta_z}{\partial y}\quad 2\psi_x+\frac{\partial\theta_z}{\partial x}\quad\frac{\partial\theta_x}{\partial y}+\frac{\partial\theta_y}{\partial x}-2\frac{\partial^2 w_0}{\partial x\,\partial y}\right] \tag{4}$$

$$\left\{\varepsilon^2\right\}^T=\left[\frac{\partial\psi_x}{\partial x}\quad\frac{\partial\psi_y}{\partial y}\quad 0\quad 3\xi_y+\frac{\partial\psi_z}{\partial y}\quad 3\xi_x+\frac{\partial\psi_z}{\partial x}\quad\frac{\partial\psi_x}{\partial y}+\frac{\partial\psi_y}{\partial x}\right]$$

$$\left\{\varepsilon^3\right\}^T=\left[\frac{\partial\xi_x}{\partial x}\quad\frac{\partial\xi_y}{\partial y}\quad 0\quad 0\quad 0\quad\frac{\partial\xi_x}{\partial y}+\frac{\partial\xi_y}{\partial x}\right]$$

## STRESS-STRAIN RELATIONSHIPS

The generalized stress-strain relations can be written in contracted notation as follows, [15]:

$$\sigma_i=Q_{ij}\varepsilon_j \qquad i,j=1,2,...6 \tag{5}$$

The transformed stress-strain relations for an orthotropic lamina oriented by an angle $\theta$ can be written as:

$$\begin{Bmatrix}\sigma_x\\ \sigma_y\\ \sigma_z\\ \tau_{yz}\\ \tau_{zx}\\ \tau_{xy}\end{Bmatrix}=\begin{bmatrix}\bar{Q}_{11} & \bar{Q}_{12} & \bar{Q}_{13} & 0 & 0 & \bar{Q}_{16}\\ \bar{Q}_{21} & \bar{Q}_{22} & \bar{Q}_{23} & 0 & 0 & \bar{Q}_{26}\\ \bar{Q}_{31} & \bar{Q}_{32} & \bar{Q}_{33} & 0 & 0 & \bar{Q}_{36}\\ 0 & 0 & 0 & \bar{Q}_{44} & \bar{Q}_{45} & 0\\ 0 & 0 & 0 & \bar{Q}_{54} & \bar{Q}_{55} & 0\\ \bar{Q}_{61} & \bar{Q}_{62} & \bar{Q}_{63} & 0 & 0 & \bar{Q}_{66}\end{bmatrix}\begin{Bmatrix}\varepsilon_x\\ \varepsilon_y\\ \varepsilon_z\\ \gamma_{yz}\\ \gamma_{zx}\\ \gamma_{xy}\end{Bmatrix} \tag{6}$$

The elements of the transformed symmetric stiffness matrix $\left[\bar{Q}\right]$ are given in [15].

During martensitic transformation of SMA the modulus of elasticity of the metal is uniformly blended with the martensite and austenite phases [3]. The SMA layer and the host layers are perfectly bonded. The constitutive relationship of the SMA layer is:

$$\{\sigma(\zeta)\} = \left[Q_s(\zeta)\right]\left(\{\varepsilon\} - \{\alpha_s\}\Delta T\right) \tag{7}$$

where $\{\alpha_s\}$ is the thermal expansion coefficient vector of the SMA layer, given as:

$$\{\alpha_s\}^T = [\alpha \quad \alpha \quad \alpha \quad 0 \quad 0 \quad 0] \tag{8}$$

where $\alpha$ is the thermal expansion coefficient of the SMA material.

$\left[Q_s(\zeta)\right]$ is the SMA layer stiffness matrix which is function of the martensite fraction, which is given in the strain-stress relation, [13, 14].

## ENERGY FORMULATION

### Hamilton's Principle

The governing differential equations of the whole structure are derived using Hamilton's principle, [15]

$$0 = \int_0^T \left(\delta U + \delta V - \delta K\right) dt \tag{9}$$

where $\delta U$ is the virtual strain energy, $\delta V$ is the virtual work done by the applied loads, and $\delta K$ is the virtual kinetic energy.

The virtual strain energy $\delta U$ is given by [15]:

$$\delta U = \int_A \left\{ \int_{-\frac{h}{2}}^{\frac{h}{2}} \left(\sigma_x \delta\varepsilon_x + \sigma_y \delta\varepsilon_y + \sigma_z \delta\varepsilon_z + \tau_{yz}\delta\gamma_{yz} + \tau_{zx}\delta\gamma_{zx} + \tau_{xy}\delta\gamma_{xy}\right) dz \right\} dxdy \tag{10}$$

or in matrix form

$$\delta U = \int_A \left\{ \int_{-\frac{h}{2}}^{\frac{h}{2}} \delta\{\varepsilon\}^T \{\sigma\} dz \right\} dxdy \tag{11}$$

By substituting for the stress components, Eq.(7), thus:

$$\delta U = \int_A \left\{ \sum_{i=1}^{k} \int_{z_{i-1}}^{z_i} \delta\{\varepsilon\}^T \left[\left[\bar{Q}\right]_i \left(\{\varepsilon\} - \{\alpha\}_i \Delta T\right)\right] dz \right\} dxdy \tag{12}$$

where $z_i$, are z-coordinates in z-direction from the mid-plane. Knowing that $\left[\bar{Q}\right]_i$ is for the core layers and $[Q_s]$ is for the SMA layers. The strain energy can be divided into two parts, as follows:

$$\delta U = \delta U_m - \delta U_T \tag{13}$$

where $\delta U_m$ and $\delta U_T$ are the mechanical, and thermal components of the strain energy defined as follows;

$$\delta U_m = \int_A \begin{Bmatrix} \delta\{\varepsilon^0\}^T [A]\{\varepsilon^0\} + \delta\{\varepsilon^0\}^T [B]\{\varepsilon^1\} + \delta\{\varepsilon^0\}^T [D]\{\varepsilon^2\} \\ +\delta\{\varepsilon^0\}^T [E]\{\varepsilon^3\} + \delta\{\varepsilon^1\}^T [B]\{\varepsilon^0\} + \delta\{\varepsilon^1\}^T [D]\{\varepsilon^1\} \\ +\delta\{\varepsilon^1\}^T [E]\{\varepsilon^2\} + \delta\{\varepsilon^1\}^T [F]\{\varepsilon^3\} + \delta\{\varepsilon^2\}^T [D]\{\varepsilon^0\} \\ +\delta\{\varepsilon^2\}^T [E]\{\varepsilon^1\} + \delta\{\varepsilon^2\}^T [F]\{\varepsilon^2\} + \delta\{\varepsilon^2\}^T [H]\{\varepsilon^3\} \\ +\delta\{\varepsilon^3\}^T [E]\{\varepsilon^0\} + \delta\{\varepsilon^3\}^T [F]\{\varepsilon^1\} + \delta\{\varepsilon^3\}^T [H]\{\varepsilon^2\} \\ +\delta\{\varepsilon^3\}^T [J]\{\varepsilon^3\} \end{Bmatrix} dxdy \tag{14}$$

where

$$\left([A],[B],[D],[E],[F],[H],[J]\right) = \sum_{i=1}^{k} \int_{z_{i-1}}^{z_i} \left[\bar{Q}\right]_i \left(1, z, z^2, z^3, z^4, z^5, z^6\right) dz \tag{15}$$

$$\delta U_T = \int_A \left\{ \delta\{\varepsilon^0\}^T \left[A^\alpha\right] + \delta\{\varepsilon^1\}^T \left[B^\alpha\right] + \delta\{\varepsilon^2\}^T \left[D^\alpha\right] + \delta\{\varepsilon^3\}^T \left[E^\alpha\right] \right\} dxdy \tag{16}$$

and

$$\left(\left[A^\alpha\right],\left[B^\alpha\right],\left[D^\alpha\right],\left[E^\alpha\right]\right) = \sum_{i=1}^{k} \int_{z_{i-1}}^{z_i} \left[\bar{Q}\right]_i \{\alpha\}_i \, \Delta T \left(1, z, z^2, z^3\right) dz \tag{17}$$

The virtual work $\delta V$ done by the applied forces can be written as, [13, 14]:

$$\delta V = \int_A \left\{ p_z(x,y)\, \delta w(x,y,t) \right\} dxdy + F_{zi}\, \delta w(x_i, y_i, t) \tag{18}$$

where $p_z(x,y)$ is the transverse distributed load, and $F_{zi}$ is the concentrated force in the z-direction at point (i).

The virtual kinetic energy $\delta K$ can be written as, [15]:

$$\delta K = \int_A \begin{pmatrix} I_0 \delta\{\dot{U}^0\}^T \{\dot{U}^0\} + I_1 \delta\{\dot{U}^0\}^T \{\dot{U}^1\} + I_2 \delta\{\dot{U}^0\}^T \{\dot{U}^2\} + I_3 \delta\{\dot{U}^0\}^T \{\dot{U}^3\} \\ +I_1 \delta\{\dot{U}^1\}^T \{\dot{U}^0\} + I_2 \delta\{\dot{U}^1\}^T \{\dot{U}^1\} + I_3 \delta\{\dot{U}^1\}^T \{\dot{U}^2\} + I_4 \delta\{\dot{U}^1\}^T \{\dot{U}^3\} \\ +I_2 \delta\{\dot{U}^2\}^T \{\dot{U}^0\} + I_3 \delta\{\dot{U}^2\}^T \{\dot{U}^1\} + I_4 \delta\{\dot{U}^2\}^T \{\dot{U}^2\} + I_5 \delta\{\dot{U}^2\}^T \{\dot{U}^3\} \\ +I_3 \delta\{\dot{U}^3\}^T \{\dot{U}^0\} + I_4 \delta\{\dot{U}^3\}^T \{\dot{U}^1\} + I_5 \delta\{\dot{U}^3\}^T \{\dot{U}^2\} + I_6 \delta\{\dot{U}^3\}^T \{\dot{U}^3\} \end{pmatrix} dxdy \tag{19}$$

where

$$(I_0, I_1, I_2, I_3, I_4, I_5, I_6) = \sum_{i=1}^{k} \int_{z_{i-1}}^{z_i} \rho_i \left(1, z, z^2, z^3, z^4, z^5, z^6\right) dz \tag{20}$$

$\{\dot{U}^0\}$, $\{\dot{U}^1\}$, $\{\dot{U}^2\}$, and $\{\dot{U}^3\}$ are given in [13, 14].

**Ritz Solution Technique**

The unknown displacements vector $\{\gamma\} = \{u_0, v_0, w_0, \theta_x, \theta_y, \theta_z, \psi_x, \psi_y, \psi_z, \xi_x, \xi_y\}$ is approximated by x-y-polynomial functions that satisfy the plate boundary conditions. Two types of boundary conditions are considered, simply-supported and cantilevered. The Ritz functions used in the present study are listed in [13, 14].

## EQUATIONS OF MOTION

The equations of motion of the plate structure are derived using the Ritz approximation technique, [13, 14]:

$$[M]\{\ddot{q}\} + [K]\{q\} = \{F\} + \{F_0\} + \{F_T\} \tag{21}$$

where $[K]$, $[M]$ are the laminated stiffness and mass matrices, $\{F\}$ and $\{F_0\}$ are the distributed and concentrated mechanical load vectors, and $\{F_T\}$ is the thermal load vector, and given by:

$$[K] = \int_A \begin{Bmatrix} \left[\bar{\varepsilon}^0\right]^T [A] \left[\bar{\varepsilon}^0\right] + \left[\bar{\varepsilon}^0\right]^T [B] \left[\bar{\varepsilon}^1\right] + \left[\bar{\varepsilon}^0\right]^T [D] \left[\bar{\varepsilon}^2\right] + \left[\bar{\varepsilon}^0\right]^T [E] \left[\bar{\varepsilon}^3\right] \\ + \left[\bar{\varepsilon}^1\right]^T [B] \left[\bar{\varepsilon}^0\right] + \left[\bar{\varepsilon}^1\right]^T [D] \left[\bar{\varepsilon}^1\right] + \left[\bar{\varepsilon}^1\right]^T [E] \left[\bar{\varepsilon}^2\right] + \left[\bar{\varepsilon}^1\right]^T [F] \left[\bar{\varepsilon}^3\right] \\ + \left[\bar{\varepsilon}^2\right]^T [D] \left[\bar{\varepsilon}^0\right] + \left[\bar{\varepsilon}^2\right]^T [E] \left[\bar{\varepsilon}^1\right] + \left[\bar{\varepsilon}^2\right]^T [F] \left[\bar{\varepsilon}^2\right] + \left[\bar{\varepsilon}^2\right]^T [H] \left[\bar{\varepsilon}^3\right] \\ + \left[\bar{\varepsilon}^3\right]^T [E] \left[\bar{\varepsilon}^0\right] + \left[\bar{\varepsilon}^3\right]^T [F] \left[\bar{\varepsilon}^1\right] + \left[\bar{\varepsilon}^3\right]^T [H] \left[\bar{\varepsilon}^2\right] + \left[\bar{\varepsilon}^3\right]^T [J] \left[\bar{\varepsilon}^3\right] \end{Bmatrix} dxdy \tag{22}$$

$$\{F_T\}^T = \int_A \left\{ \left[\bar{\varepsilon}^0\right]^T \left[A^\alpha\right] + \left[\bar{\varepsilon}^1\right]^T \left[B^\alpha\right] + \left[\bar{\varepsilon}^2\right]^T \left[D^\alpha\right] + \left[\bar{\varepsilon}^3\right]^T \left[E^\alpha\right] \right\} dxdy \tag{23}$$

$$\begin{aligned} \{F\}^T &= \int_A \left[ 0 \quad 0 \quad p_z(x,y) \{a_3\}^T \quad 0 \quad 0 \quad 0 \quad 0 \quad 0 \quad 0 \quad 0 \quad 0 \right] dxdy \\ \{F_0\}^T &= \left[ 0 \quad 0 \quad F_{zi} \{a_3(x_i, y_i)\}^T \quad 0 \quad 0 \quad 0 \quad 0 \quad 0 \quad 0 \quad 0 \quad 0 \right] \end{aligned} \tag{24}$$

$$[M] = \int_A \begin{pmatrix} I_0 \delta \left[\bar{U}^0\right]^T \left[\bar{U}^0\right] + I_1 \delta \left[\bar{U}^0\right]^T \left[\bar{U}^1\right] + I_2 \delta \left[\bar{U}^0\right]^T \left[\bar{U}^2\right] + I_3 \delta \left[\bar{U}^0\right]^T \left[\bar{U}^3\right] \\ + I_1 \delta \left[\bar{U}^1\right]^T \left[\bar{U}^0\right] + I_2 \delta \left[\bar{U}^1\right]^T \left[\bar{U}^1\right] + I_3 \delta \left[\bar{U}^1\right]^T \left[\bar{U}^2\right] + I_4 \delta \left[\bar{U}^1\right]^T \left[\bar{U}^3\right] \\ + I_2 \delta \left[\bar{U}^2\right]^T \left[\bar{U}^0\right] + I_3 \delta \left[\bar{U}^2\right]^T \left[\bar{U}^1\right] + I_4 \delta \left[\bar{U}^2\right]^T \left[\bar{U}^2\right] + I_5 \delta \left[\bar{U}^2\right]^T \left[\bar{U}^3\right] \\ + I_3 \delta \left[\bar{U}^3\right]^T \left[\bar{U}^0\right] + I_4 \delta \left[\bar{U}^3\right]^T \left[\bar{U}^1\right] + I_5 \delta \left[\bar{U}^3\right]^T \left[\bar{U}^2\right] + I_6 \delta \left[\bar{U}^3\right]^T \left[\bar{U}^3\right] \end{pmatrix} dxdy \tag{25}$$

## SMA CONSTITUTIVE MODELS

### SMA Linear Model

The linear model provides a one-dimensional relation between the martensite fraction with temperature and stress during the phase transformation, [8]. In the present model the heating and cooling transition process is reproduced in Eq.(26) and Eq.(27) respectively:

$$\zeta = 1 - \frac{T - A_s}{A_f - A_s} + \frac{|\sigma|}{C_A (A_f - A_s)} \tag{26}$$

$$\zeta = 1 - \frac{T - M_f}{M_s - M_f} + \frac{|\sigma|}{C_M (M_s - M_f)} \tag{27}$$

where $C_A$ and $C_M$ are the material constants which indicate the influence of the stress on the phase transformation temperatures. $A_s$ and $A_f$ are the start and finish temperatures of the phase transformation from martensite to austenite, respectively. $M_s$ and $M_f$ are the start and finish temperatures of the phase transformation from austenite to martensite, respectively. $\sigma$ is the magnitude of the stress in the SMA layer, which is assumed to be the hydrostatic stress, $|\sigma| = (\sigma_x + \sigma_y + \sigma_z)/3$.

### SMA Brinson's Model

The Brinson's model [12] made a significant improvement over Tanaka's model [9, 11], and the Liang and Rogers's model [10]. It recognizes the stress induced martensite (SIM) as the only martensite that gives the functional property of shape memory effect (SME) and pseudo elasticity rather than the total martensite that contains both the temperature induced martensite (TIM) and the stress induced martensite (SIM). Brinson's model assumes that the transformation depends only on the temperature and the stress, and the amount of transformation that occurs is described using the volume fraction of the stress induced martensite, $\xi_S$. Brinson's model is quite popular for engineering applications since it is simple, accurate and easy to implement into numerical applications.

Brinson made a modification so that this model can be used at low temperatures by dividing the martensitic volume fraction into two parts:

$$\xi = \xi_S + \xi_T \tag{28}$$

where $\xi_S$ corresponds to the fraction of the stress induced martensite (SIM) and $\xi_T$ refers to the fraction of the temperature induced martensite (TIM). From Tanaka [9] and Eq.(28), the stress can be expressed as:

$$\sigma = \sigma(\varepsilon, \xi_S, \xi_T, T) \tag{29}$$

After a simple derivation and applying a force condition we get the constitutive relationship of Brinson's model for constant material parameter [11]:

$$\sigma-\sigma_0=D(\varepsilon-\varepsilon_0)+\Omega(\xi_S-\xi_{S0})+\theta(T-T_0) \tag{30}$$

where D is the Young Modulus, θ is the thermoelastic tensor and Ω is the transformation tensor. The effect of stress on the transition temperature now must consider the conversion of TIM to SIM. This process of conversion starts after a TIM is given a stress up to a critical value, $\sigma_s^{cr}$ , and ends at a stress value of, $\sigma_f^{cr}$ . The values of these critical stresses can be determined through experiments, or theoretically by developing a model based on the potential energy necessary to overcome the chemical energy barrier for conversion of twins as in the work of Achenbach and Muller [16]. The stress temperature coefficients, $C_A$ and $C_M$ in Brinson's model are not assumed to be equal, and are both determined through experiments. The evolution equations are listed in Ref. [11], Appendix (A).

## HEAT TRANSFER

### Heat Equations Modeling of SMA Layer

The SMA layer is activated when exposed to heat. Heat power is considered as a homogeneous heat source in the SMA layer. The thermal energy of the activated SMA layer is assumed to be lost by conduction through the core structure. A two-dimensional temperature distribution is considered. Considering a dx-dy element of the SMA layer, the energy balance equation can be given as, [5]:

$$C_s\frac{\partial T}{\partial t}-Q_s\frac{\partial \zeta}{\partial t}-k_s\frac{\partial^2 T}{\partial x^2}-k_s\frac{\partial^2 T}{\partial y^2}+K_e\left(T-T_{\text{sink}}\right)-P=0 \tag{31}$$

where $C_s\left(\partial T/\partial t\right)$ is the rate of change in the internal energy of the SMA layer. $C_s=\rho_s c_s$, in which $\rho_s$ and $c_s$ are the density in $\left[kgm^{-3}\right]$, and the specific heat in $\left[J\,kg^{-1}{}^{\circ}C^{-1}\right]$, respectively. $-Q_s\left(\partial\zeta/\partial t\right)$ is the rate of energy contributed to the phase transformation of the SMA layer. Here $Q_s=\rho_s q_s$ and $q_s$ is the heat of transition in $\left[J\,kg^{-1}\right]$. $-k_s\left(\partial^2 T/\partial x^2\right)-k_s\left(\partial^2 T/\partial y^2\right)$ is the rate of heat conduction in the x and y directions through the SMA layer, and $k_s$ is the thermal conductivity in $\left[Wm^{-1}{}^{\circ}C^{-1}\right]$. $K_E\left(T-T_{\text{sink}}\right)$ is the quasi-steady model for the heat lost by conduction through the core layer, when the core heat capacity is neglected, [17]. $K_E=k_e/\left[t_s\left(h-t_s\right)\right]$, [5], where $k_e$ is the thermal conductivity of the core layers in $\left[Wm^{-1}{}^{\circ}C^{-1}\right]$. $T$ and $T_{\text{sink}}$ are the temperatures in $\left[{}^{\circ}C\right]$ of the SMA layer and the heat sink, which has a constant temperature and bonded to the lower surface of the core.

$P$ is the input heat power density in $\left[W/m^3\right]$ generated by the electric current passed though the SMA layer in the heating process. $P$ is zero if Eq.(31) is applied to the cooling process. $t$ is the time in $\left[\text{sec}\right]$.

Equation (31) may be written in dimensionless form as:

$$\frac{\partial\theta}{\partial\tau}-R_{MA}\frac{\partial\zeta}{\partial\tau}-\frac{\partial^2\theta}{\partial X^2}-\frac{\partial^2\theta}{\partial Y^2}+R_k\left(\theta-S\right)-R_P=0 \tag{32}$$

where $\theta$ is the non-dimensional temperature of the SMA, $\tau$ is the dimensionless time, $R_{MA}$ is the dimensionless heat of transition of the SMA, $R_k$ is the dimensionless thermal conductivity of the core, $S$ is the heat sink strength which characterizes the heat conduction loss from the SMA through the core to the heat sink, and $R_P$ is the dimensionless input power to the SMA layer. The dimensionless symbols are defined in Appendix (B).

**Heat Equations Solution**

The variational formulation of Eq.(32) over the plate area $\Omega$ is obtained by multiplying the equation by a weight function $N_i$

$$\int_\Omega N_i\left\{\frac{\partial\theta}{\partial\tau}-R_{MA}\frac{\partial\zeta}{\partial\tau}-\frac{\partial^2\theta}{\partial X^2}-\frac{\partial^2\theta}{\partial Y^2}+R_k\left(\theta-S\right)-R_P\right\}dXdY=0 \tag{33}$$

Integrating by parts and rearranging the equation elements:

$$\begin{aligned}&\int_\Omega\left\{N_i\frac{\partial\theta}{\partial\tau}-N_i R_{MA}\frac{\partial\zeta}{\partial\tau}-\frac{\partial N_i}{\partial X}\frac{\partial\theta}{\partial X}-\frac{\partial N_i}{\partial Y}\frac{\partial\theta}{\partial Y}+N_i R_k\left(\theta-S\right)-N_i R_P\right\}dXdY\\&\quad=\int_\Gamma N_i\left(\frac{\partial\theta}{\partial X}n_x-\frac{\partial\theta}{\partial Y}n_y\right)ds\end{aligned} \tag{34}$$

where $n_x$ and $n_y$ are the direction cosines of the boundary surface in the x and y directions. The variables $\theta$ and $\zeta$ are approximated over the plate by the following interpolation functions:

$$\begin{aligned}\theta&=\sum_{i=1}^{4}N_i\left(X,Y\right)\bar{\theta}_i\left(\tau\right)\\\zeta&=\sum_{i=1}^{4}N_i\left(X,Y\right)\bar{\zeta}_i\left(\tau\right)\end{aligned} \tag{35}$$

where $N_i\ (i=1,2,3,4)$ are the linear interpolation functions of the plate in x-y directions. $\bar{\theta}_i$ and $\bar{\zeta}_i$ are the unknown temperature and martensite fraction coefficients, respectively. By substituting Eq.(35) in Eq.(34), thus:

$$\left[C^1\right]\left\{\frac{\partial\bar{\theta}}{\partial\tau}\right\}+\left[C^2\right]\left\{\bar{\theta}\right\}+\left[C^3\right]\left\{\frac{\partial\bar{\zeta}}{\partial\tau}\right\}=\left\{F^{th}\right\} \tag{36}$$

where

$$C_{ij}^{1}=\int_{\Omega}N_{i}N_{j}dXdY$$

$$C_{ij}^{2}=\int_{\Omega}\left\{\frac{\partial N_{i}}{\partial X}\frac{\partial N_{j}}{\partial X}+\frac{\partial N_{i}}{\partial Y}\frac{\partial N_{j}}{\partial Y}+R_{k}N_{i}N_{j}\right\}dXdY$$

$$C_{ij}^{3}=-\int_{\Omega}R_{MA}N_{i}N_{j}dXdY$$

$$F_{i}^{th}=\int_{\Omega}\left(R_{P}-R_{k}S\right)N_{i}dXdY+\int_{\Gamma}N_{i}\left(\frac{\partial\bar{\theta}}{\partial X}n_{x}-\frac{\partial\bar{\theta}}{\partial Y}n_{y}\right)ds$$

α-family method is used to transfer Eq.(36) from ordinary differential equations to a set of algebraic equations, in which a weighted average of the time derivative of a dependent variable is approximated at two consecutive time steps by linear interpolation of the values of the variable at the two steps.

For different values of α (0<α<1), a numerical integration schemes can be obtained [18].

Assuming constant time step $\Delta t$ gives:

$$\alpha\left\{\frac{\partial\bar{\theta}}{\partial\tau}\right\}^{n+1}+(1-\alpha)\left\{\frac{\partial\bar{\theta}}{\partial\tau}\right\}^{n}=\frac{\left\{\bar{\theta}\right\}^{n+1}-\left\{\bar{\theta}\right\}^{n}}{\Delta\tau} \tag{37}$$

Rearranging terms of Eq.(36) gives:

$$\begin{aligned}\left(\left[C^{1}\right]+\Delta\tau\alpha\left[C^{2}\right]\right)\left\{\bar{\theta}\right\}^{n+1}=&\left(\left[C^{1}\right]-(1-\alpha)\Delta\tau\left[C^{2}\right]\right)\left\{\bar{\theta}\right\}^{n}\\&+\Delta\tau\left(\alpha\left\{F^{th}\right\}^{n+1}+(1-\alpha)\left\{F^{th}\right\}^{n}\right)\\&-\Delta\tau\left[C^{3}\right]\left(\alpha\left\{\frac{\partial\bar{\zeta}}{\partial\tau}\right\}^{n+1}+(1-\alpha)\left\{\frac{\partial\bar{\zeta}}{\partial\tau}\right\}^{n}\right)\end{aligned} \tag{38}$$

Knowing that;

$$\Delta\tau\left(\alpha\left\{\frac{\partial\bar{\zeta}}{\partial\tau}\right\}^{n+1}+(1-\alpha)\left\{\frac{\partial\bar{\zeta}}{\partial\tau}\right\}^{n}\right)=\left\{\bar{\zeta}\right\}^{n+1}-\left\{\bar{\zeta}\right\}^{n} \tag{39}$$

Eq.(38) can be written in a set of algebraic equations as follows:

$$\left[\hat{K}\right]\left\{\bar{\theta}\right\}^{n+1}=\left\{\hat{F}\right\} \tag{40}$$

where

$$\left[\hat{K}\right]=\left(\left[C^{1}\right]+\Delta\tau\alpha\left[C^{2}\right]\right)$$

and

$$\left\{\hat{F}\right\}=\left(\left[C^{1}\right]-(1-\alpha)\Delta\tau\left[C^{2}\right]\right)\left\{\bar{\theta}\right\}^{n}+\Delta\tau\left\{F^{th}\right\}-\left[C^{3}\right]\left(\left\{\bar{\zeta}\right\}^{n+1}-\left\{\bar{\zeta}\right\}^{n}\right)$$

While performing the iteration process, an estimate value for the martensite fraction unknown coefficient $\{\bar{\zeta}\}_{est}^{n+1}$ should be calculated at $t_{n+1}$ in order to calculate $\{\hat{F}\}$. Using Eq.(26) and Eq.(27) $\{\bar{\zeta}\}_{est}^{n+1}$ can be calculated by the free response model:

$$\zeta_{est}^{n+1} = 1 - \theta_{est}^{n+1} \tag{41}$$

where $\theta_{est}^{n+1}$ is obtained by replacing the term $\left\{\frac{\partial \bar{\zeta}}{\partial \tau}\right\}$ by $\left\{-\frac{\partial \bar{\theta}}{\partial \tau}\right\}$ in Eq.(36). Thus, $\theta_{est}^{n+1}$ can be determined by solving the following set of algebraic equations:

$$[K']\{\bar{\theta}\}_{est}^{n+1} = \{F'\} \tag{42}$$

where

$$[K'] = \left(\left[C^1\right] - \left[C^3\right] + \Delta\tau\alpha\left[C^2\right]\right)$$

and

$$\{F'\} = \left(\left[C^1\right] - \left[C^3\right] - (1-\alpha)\Delta\tau\left[C^2\right]\right)\{\bar{\theta}\}^n + \Delta\tau\{F^{th}\}$$

## SOLUTION PROCEDURE

1- Select initial values for $\theta^0$ and $\zeta^0$ and solve Eq. (40) for the initial deformation $\{q\}^0$ and initial stresses $\{\sigma\}^0$ of the plate due to mechanical loading.

2- Calculate the new time $t_{n+1} = t_n + \Delta t$ and estimate the martensite fraction $\zeta_{est}^{n+1}$ at $t_{n+1}$ by the free response model Eq.(41) where $\theta_{est}^{n+1}$ is obtained by solving Eq.(42).

3- Solve Eq. (40) for $\{q\}^{n+1}$ and $\{\sigma\}^{n+1}$ based on $\{q\}^0$ and $\zeta_{est}^{n+1}$.

4- Calculate $\zeta^{n+1}$ using either linear or Brinson's SMA constitutive models Eq.(26) and Eq.(27) or Eq.(28), based on $\{\sigma\}^{n+1}$.

5- Check convergence by testing the value $\left(\zeta^{n+1} - \zeta_{est}^{n+1}\right)$. If the convergence criterion is satisfied, repeat the above steps with a time increment $\Delta t$. If the convergence criterion is not satisfied, calculate the new estimated $\zeta_{est}^{n+1}$ by using relaxation method $\zeta_{est}^{n+1} = \zeta^{n+1} + \lambda\left(\zeta^{n+1} - \zeta_{est}^{n+1}\right)$ where $\lambda$ is the minimum eigenvalue given by $\lambda \le (2/\Delta t)$ [3].

## NUMERICAL RESULTS AND DISCUSSION

The static and dynamic deformation of the core structure are given in Refs. [13, 14]. To verify the present thermal model, two cases are presented. Case (I) studies the stress-free thermal response of SMA laminated plate, while the phase transformation

response of a cantilever plate subjected to mechanical and thermal loads is considered in case (II). Parametric studies are then presented in case (III) to investigate the effect of plate thickness, aspect ratio, material properties, thermal expansion coefficient, and shape memory alloy sheet thickness on the transverse deflections, natural frequencies, and shape memory alloy's response time. Simply supported plates and cantilever plates are used in these cases. A set of computer programs was developed, for this investigation, using Mathematica 7.

**Case (I): Free Thermal Response of SMA Laminated Plate**

The plate consists of 55-Nitinol for the SMA layer glued on the top of Dow Corning SYLGARD core. The SMA layer thickness $t_s = 0.25\times10^{-3}m$, and an core layer thickness $(h - t_s) = 2.25\times10^{-3}m$. The total plate thickness is $h = 2.5\times10^{-3}m$. The plate dimensions are taken as $a = b = 0.25m$. The material properties are given in Table 1 [3, 17].

**Table 1.** Material properties for SMA and plate core [3, 17].

| Property | SMA (55-Nitinol) | Elastomer Sylgard |
|---|---|---|
| Density, $\rho\left[kg/m^3\right]$ | 6500 | 1050 |
| Specific heat, $c\ [J/(kg\,°C)]$ | 883 | 1422 |
| Thermal conductivity, $k\ [W/(m\,°C)]$ | 17 | 0.146 |
| Thermal expansion coefficient, $\alpha\left[°C^{-1}\right]$ | $23\times10^{-6}$ | |
| Heat of transition, $q_s\left[J/kg\right]$ | 12600 | |
| Material constant, $C_A\ [MPa/°C]$ | 10.3 | |
| Material constant, $C_M\ [MPa/°C]$ | 10.3 | |
| Young's modulus of core, $E_c\ [MPa]$ | | 1300 |
| Young's modulus in martensite phase, $E_M\ [MPa]$ | 26300 | |
| Young's modulus in austenite phase, $E_A\ [MPa]$ | 67000 | |
| Poisson's ratio, $\nu$ | 0.3 | 0.3 |
| Martensite start temperature, $M_s\ [°C]$ | 18.4 | |
| Martensite finish temperature, $M_f\ [°C]$ | 9 | |
| Austenite start temperature, $A_s\ [°C]$ | 34.5 | |
| Austenite finish temperature, $A_f\ [°C]$ | 49 | |

If we assume for validation purpose that $A_f - A_s = M_s - M_f = 10°C$ [17], then for 55-Nitinol $R_{ma} = 1.4$.

The response time of the actuator of the SMA layer for martensite-to-austenite heating transition for an applied power $P = 7.787\times10^{7}W\ /m^{3}\ (R_p = 0.2863)$, and for austenite-to-martensite cooling transition for a sink temperature $T_{\sin k} = -21℃\ \ (S = 3)$ are shown in Table. 2 for both linear and Brinson's SMA model and compared with Wirtz, [17]. The response time is also calculated from the conservation of thermal energy in the SMA layer from basic heat transfer equation [19],

$$Q_{generated} = Q_{body} + Q_{dissipated} \tag{43}$$

**Table. 2.** Response time of the actuator**.**

| Model | | Present (linear SMA model) | Present (Brinson's SMA model) | Basic heat transfer equations, [19] | Wirtz, [17] |
|---|---|---|---|---|---|
| Heating response | time [sec.] | 17.83 | 18.99 | 17.89 | 20.9 |
| | τ | 8.45 | 9 | 8.48 | 9.9 |
| Cooling response | time [sec.] | 15.5 | 15.5 | 15.46 | 15.5 |
| | τ | 7.35 | 7.35 | 7.32 | 7.36 |

**Case (II): Phase Transformation of SMA Laminated Plate**

The phase transformation response of SMA layer located at the top, subjected to a uniformly distributed load, $q = -1000N/m^{2}$ and input heating power $P = 5.6\times10^{8}W/m^{3}$ is studied. The plate dimensions are $a = 0.25m$, $b = 0.14m$ with five layers for the core of thickness $1\times10^{-3}m$ each. The thickness of the SMA layer is $0.05\times10^{-3}m$. The time step $\Delta t = 0.01\sec$ is used. The material properties are given in Table 1 [3].

The variations in martensite fraction in the activated SMA layer using the linear and Brinson's models are shown in Figure 2. in comparison with the results obtained by Balapgol [3], and Ghomshei [2]. A good agreement is found between the proposed model and the mentioned references results.

**Case (III): Parametric Study of SMA Composite Plate**

The plate used in case (I) is used for such parametric studies. The plate thickness is divided into ten layers, the top layer is SMA, and the remaining nine layers form the plate core. The material properties are given in Table 1 and the plate dimensions are shown in Figure 3. The plate span is $a = 100\,\mathrm{mm}$, width $b = 25\,\mathrm{mm}$, and thickness $h = 3\,\mathrm{mm}$. The thickness of the SMA layer is $t_s = 0.3\,\mathrm{mm}$. The plate is assumed to be thermally insulated on all four edges. The plate carries a downward load $F_z = 20\ \mathrm{N}$ at the free end. The value of dimensionless time interval $\Delta\tau = 0.1$ is selected.

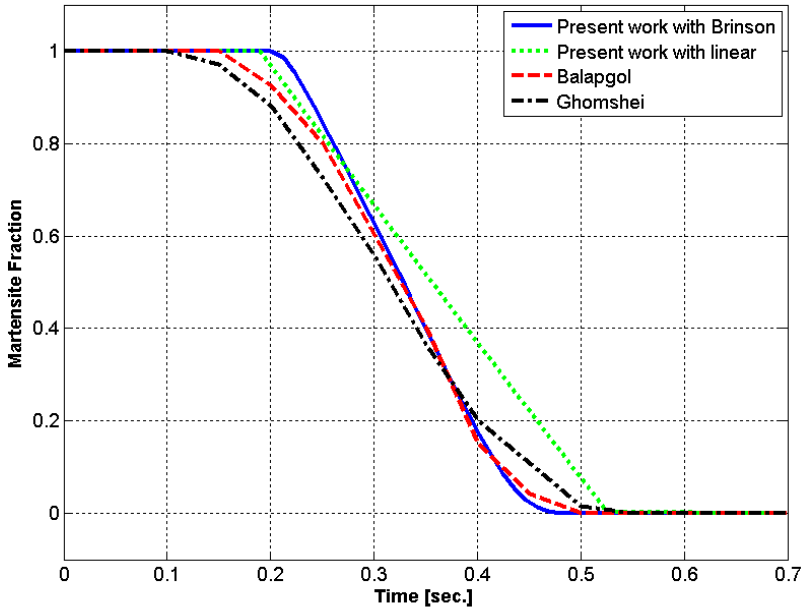


**Figure 2.** Variation of martensite fraction ( $\zeta$ ) in activated SMA layer**.**

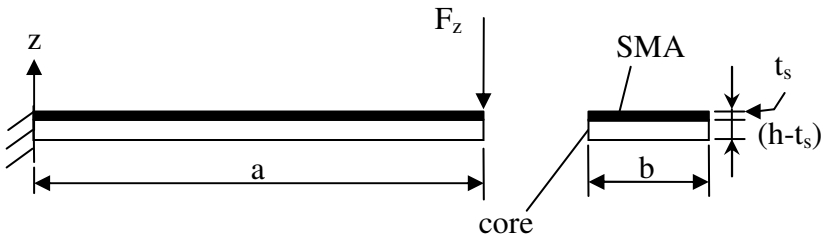


**Figure 3.** SMA laminated cantilever plate**.**

An input heat power $P = 2\times10^7 W/m^3$ is used in the heating phase, and the sink temperature is $T_{\sin k} = -20°C$ through the whole heating-cooling cycle.

As the first step the deflection response is calculated neglecting the effect of thermal expansion of the SMA layer. Then it is calculated considering the thermal expansion effect on the SMA layer only because the core layer is assumed at a constant temperature equal to the sink temperature, and the heating is only on the SMA layer.

Figure 4 shows the temperature response of the given plate in the heating-cooling cycle with input heat power $P = 2\times10^7 W/m^3$ applied until reaching the austenite-finish temperature ($A_f$). Figure 5 shows the variation of the martensite fraction with the response time of the plate in the heating-cooling cycle. While heating from $A_s$ to $A_f$ the SMA layer is transformed from fully martensite phase to fully austenite phase.

This is an endothermic process, which absorbs part of the input heat causing decrease in the heating rate of the SMA layer as seen in Fig. 4. This transformation also causes reduction of the martensite fraction from 1 at $A_s$ to 0 at $A_f$ as shown in

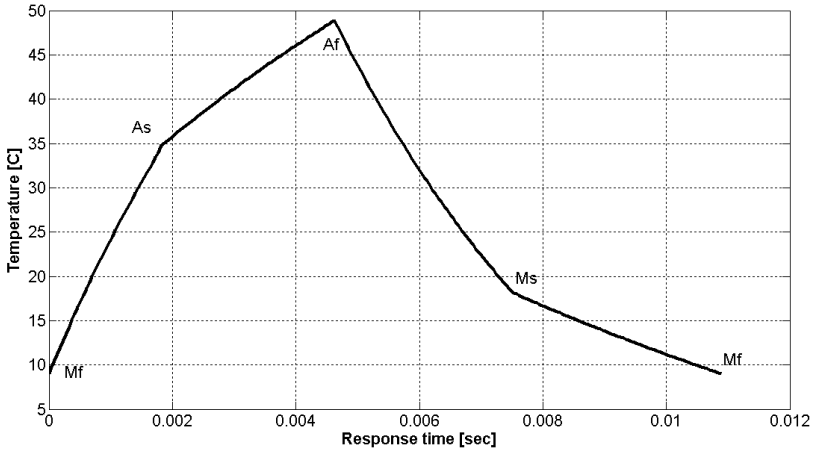


**Figure 4.** Temperature response of the SMA laminated cantilever plate in the heating-cooling cycle with input power $P = 2\times10^{7} W/m^{3}$

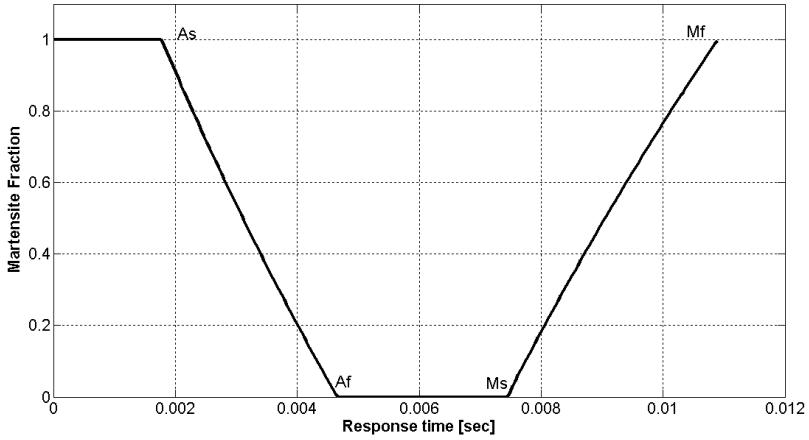


**Figure 5.** Variation of the martensite fraction with time response of the plate in the heating-cooling cycle with input power $P = 2\times10^{7} W/m^{3}$

Figure 5. While cooling from $M_s$ to $M_f$ the SMA layer is transformed from fully austenite phase to fully martensite phase. This is an exothermic process, which emits heat, causing decrease in the cooling rate of the SMA layer as seen in Figure 4. This transformation then increases the martensite fraction from 0 at $M_s$ to 1 at $M_f$, as seen in Figure 5.

Figure **6** gives the lateral deflection of the plate at y=b/2 before activation ($T<M_f$) and after activation ($T>A_f$), the core Young's modulus is 13 GPa. It is clear that the lateral deflection of the plate is decreased with the activation of the SMA layer due to the increase of its Young's modulus from $E_M$ in the martensite phase to $E_A$ in the austenite phase as given in Table 1.

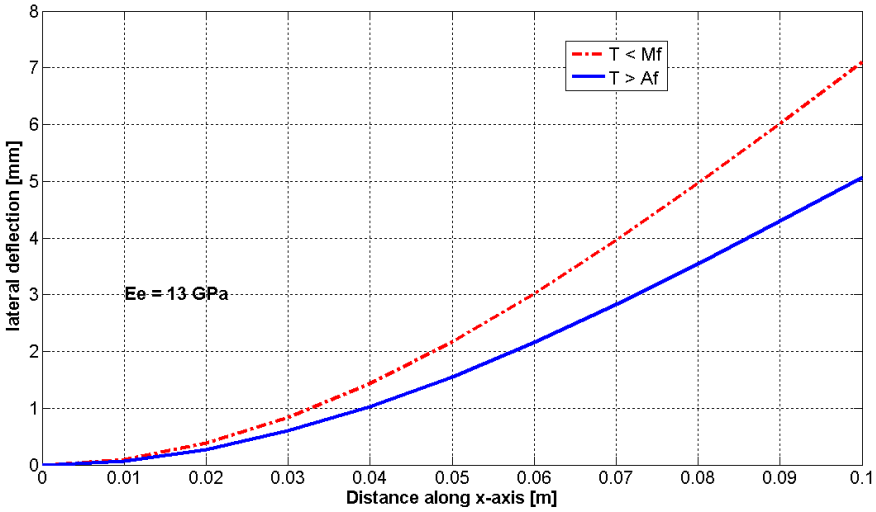


**Figure 6.** Lateral deflection of the plate before activation ($T<M_f$) and after activation ($T>A_f$).

## (1) Effect of Young's modulus of plate core ($E_c$)

To study the effect of Young's modulus of core ($E_c$) on the lateral deflection of SMA laminated cantilever plate, $E_e$ is changed from 10 to 80 GPa. Figures 7 and 8 show the lateral deflection of the plate before activation ($T<M_f$) and after activation ($T>A_f$), respectively, at different values of $E_c$. Figure 9 shows the effect of Young's modulus of core ($E_c$) on the dimensionless response time and maximum deflection of SMA laminated cantilever plate at the middle point of the free end. Figure 10 shows the effect of Young's modulus of core ($E_c$) on the response time and the natural frequency of the plate.

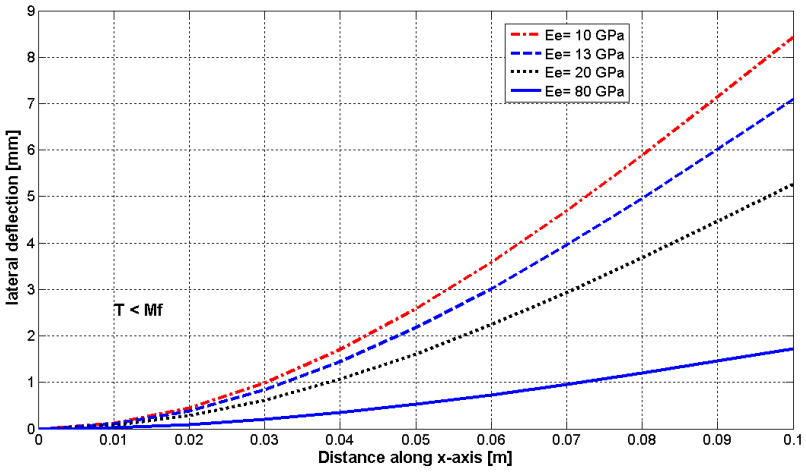


**Figure 7.** Effect of Young's modulus of core ($E_c$) on the Lateral deflection of the plate before activation ($T<M_f$).

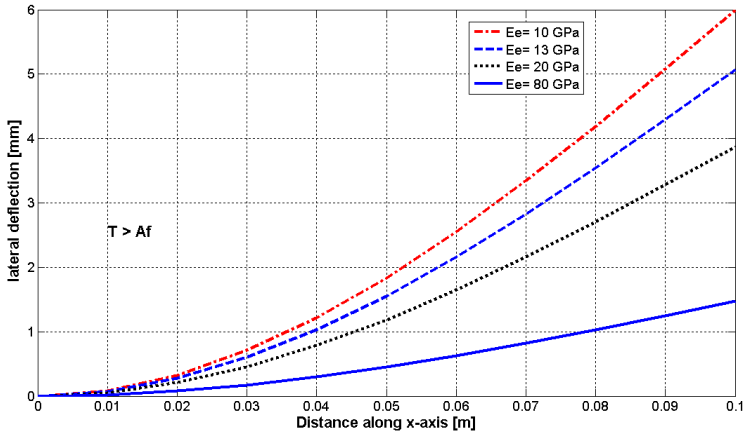


**Figure 8.** Effect of Young's modulus of core ($E_c$) on the Lateral deflection of the plate after activation ($T>A_f$).

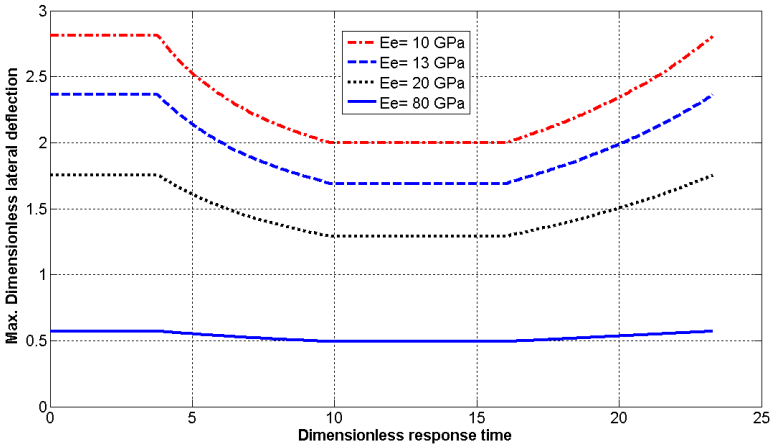


**Figure 9.** Effect of Young's modulus of core ($E_c$) on the dimensionless response time and the maximum dimensionless deflection ($\bar{w} = w/h$) of the plate at the middle of the free end (x=a and y=b/2).

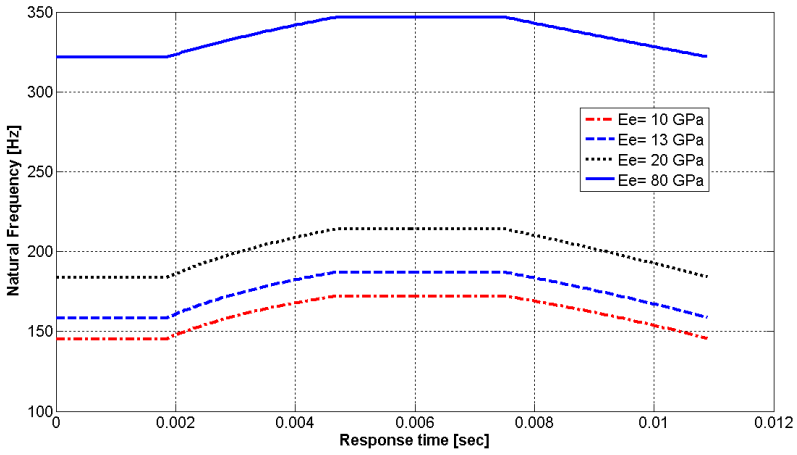


**Figure 10.** Effect of Young's modulus of core ($E_c$) on the response time and natural frequency of the plate**.**

**(2) Effect of SMA thermal expansion**

The lateral deflection is decreased in the heating stage, and increased in the cooling stage. The temperature of the SMA layer is varied in the heating-cooling cycle as illustrated in Figure 4, while the temperature of the core layer is considered constant.

Figure 11 shows the lateral deflection of SMA laminated cantilever plate before and after with and without thermal expansion effect. It is clear that the activation decreases the deflection, and taking the thermal expansion effect into consideration adds an additional decrease of the deflection. While Figure 12 shows the effect of thermal expansion on the response time and the deflection of the cantilever plate at the free end. It is clear that the thermal expansion decreases the deflection without affecting the time response.

The reason of that is that at the staring temperature ($M_f$) the SMA layer is at martensite phase. Applying the transverse load in the positive z-direction causes the plate to be deformed upwards. While heating form $M_f$ to $A_s$ the temperature of the SMA layer increases as seen in Figure 4 which causes the SMA layer to expand. Since this layer is positioned at a distance above the mid-plane, its expansion will produce an axial force above the neutral axis, which acts as a moment that forces the plate to deform downward to decrease the deformation gradually with heating under the same applied transverse load.

Thus heating from $M_f$ to $A_s$ has no effect on the SMA phase, it is still at martensite phase. The decrease in deformation is due to thermal expansion only. Once the temperature reaches $A_s$ the SMA layer starts to transform from martensite phase to austenite phase, which means gradual increase in the modulus of elasticity of the SMA layer and the total stiffness of the plate and subsequently causes a gradual decrease in the plate deflection until the temperature reaches $A_f$.

After the plate is completely transformed to the austenite phase, it has the minimum deflection reached in the heating cycle. At $A_f$, no more heating power is added and the heat sink decreases the temperature gradually. Cooling from $A_f$ to $M_s$ will not affect the SMA layer phase, but will cause thermal contraction. This contraction produces an axial compression force positioned above the neutral axis, which acts as a moment that forces the plate to deflect upwards, which means that the deflection increases gradually while cooling.

The cooling after $M_s$ causes the SMA layer to be transformed to austenite phase, this gradually decreases the modulus of elasticity from $E_A$ to $E_M$. Thus, the total stiffness of the plate also decreases causing more deflection under the same applied transverse load. The heat cycle is finished at $M_f$, while the deflection has the maximum value.

It is obvious that if the transverse load is downward or the SMA layer is positioned at the bottom of the plate, the thermal expansion effect will be inverted. This means that heating increases deflection and cooling decreases deflection.

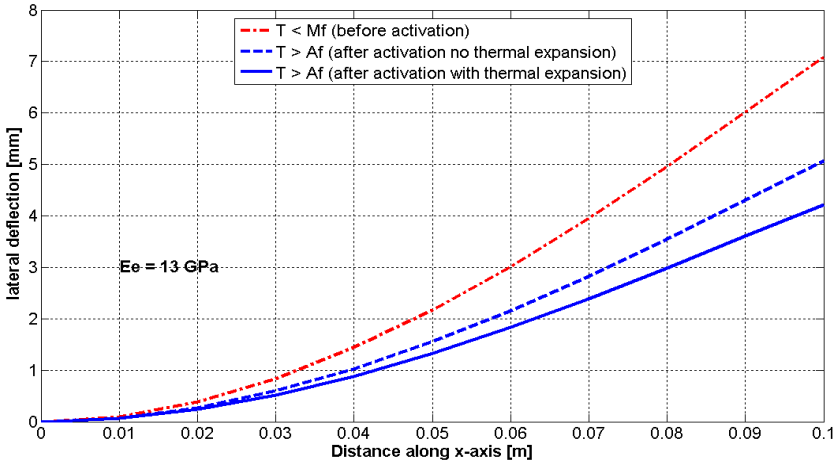


**Figure 11.** Lateral deflection of SMA laminated cantilever plate before activation ($T<M_f$) and after activation ($T>A_f$) with and without thermal expansion effect**.**

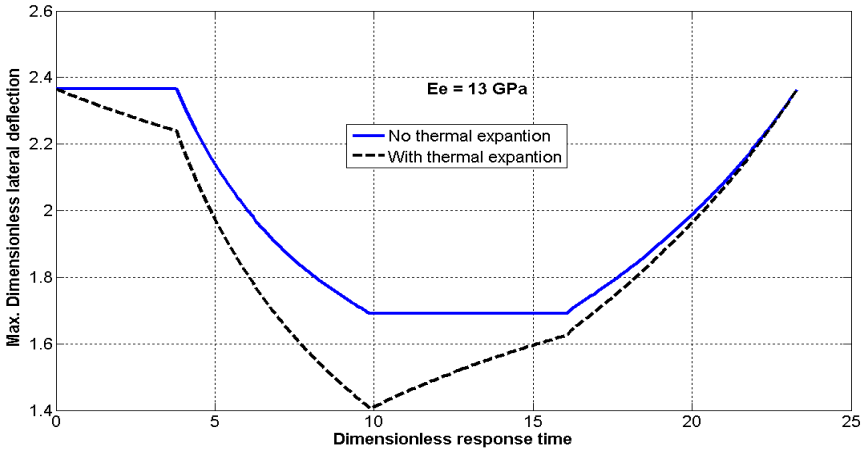


**Figure 12.** Effect of thermal expansion on the dimensionless response time and the maximum dimensionless deflection ($\overline{w} = w/h$ ) of SMA laminated cantilever plate at free end (x=a and y=b/2).

Figure 13 shows the effect of Young's modulus of core ($E_c$) on the lateral deflection of the plate after activation ($T>A_f$) with thermal expansion effect. Figure 14 presents the effect of Young's modulus of core ($E_c$) on the response time and the maximum deflection of the plate at the middle of the plate free end with thermal expansion effect.

### (3) Effect of the SMA layer thickness

The effect of the SMA layer thickness on the response time, plate deflection and natural frequency, a plate with the same value of the total thickness h=3mm, four values of SMA layer thickness ($t_s$) are chosen such that ($t_s$/h= 0.1, 0.2, 0.3, 0.4). Figure 15 shows SMA thickness effect on the temperature response of the plate in the heating-cooling cycle.

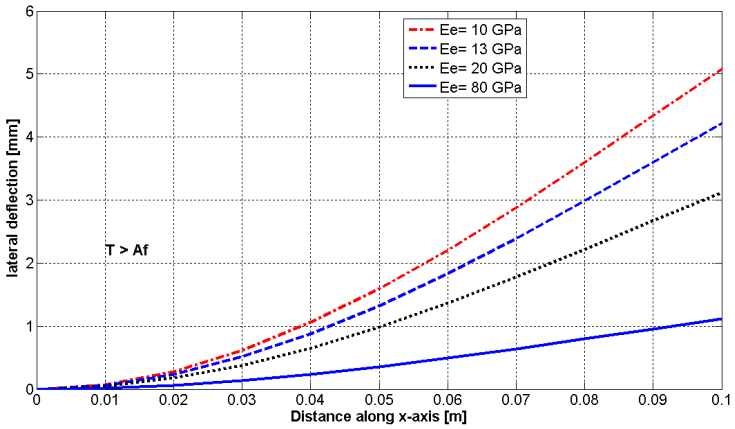


**Figure 13.** Effect of Young's modulus of core ($E_c$) on the Lateral deflection after activation ($T>A_f$) with thermal expansion effect**.**

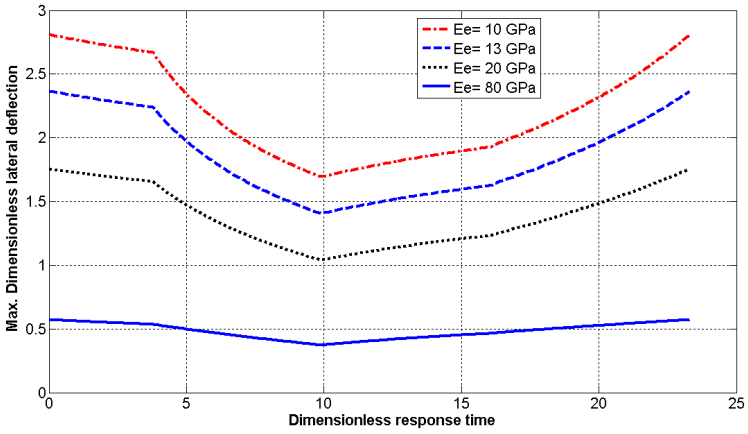


**Figure 14.** Effect of Young's modulus of core ($E_c$) on the dimensionless response time and the maximum dimensionless deflection ($\bar{w} = w/h$ ) of the plate at free end (x=a and y=b/2) with thermal expansion effect.

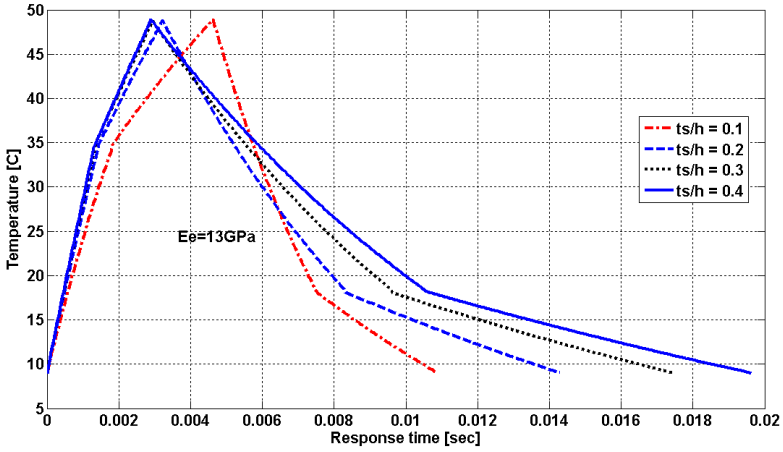


**Figure 15.** SMA thickness effect on the temperature response of the SMA layer in the heating-cooling cycle with input power $P = 2\times10^7 W/m^3$

Figure 17 shows the SMA thickness effect on the variation of the martensite fraction with response time of the SMA laminated cantilever plate in the heating-cooling cycle. Increasing the SMA layer thickness will decrease and increase the response time during heating and cooling, respectively. Actually increasing the SMA thickness ($t_s$) with the same total thickness (h), means decreasing the core thickness ($t_e$). Both ($t_s$) and ($t_e$) affect the time response. As seen in the energy balance equation Eq. (31) , the only term affected with the change of ($t_s$) and ($t_e$) is $K_E\left(T-T_{\text{sink}}\right)$, which represents the heat lost by conduction through the core layer such that $K_E = k_e/\left(t_s t_e\right)$, where $k_e$ is the thermal conductivity of the core in $\left[Wm^{-1}{}^{\circ}C^{-1}\right]$. It is clear that the cooling rate is inversely proportional to $\left(t_s t_e\right)$. Figure 17 shows the relation between $K_E$ and the SMA thickness ratio $(t_s/h)$. It is clear that $K_E$ decreases until the SMA thickness becomes equal to the core thickness $(t_s/h)=0.5$, then $K_E$ increases again. This explains the increase in the heating rate and the decrease in the cooling rate with increasing the SMA thickness ratio $(t_s/h)$ , as shown in Figure 15.

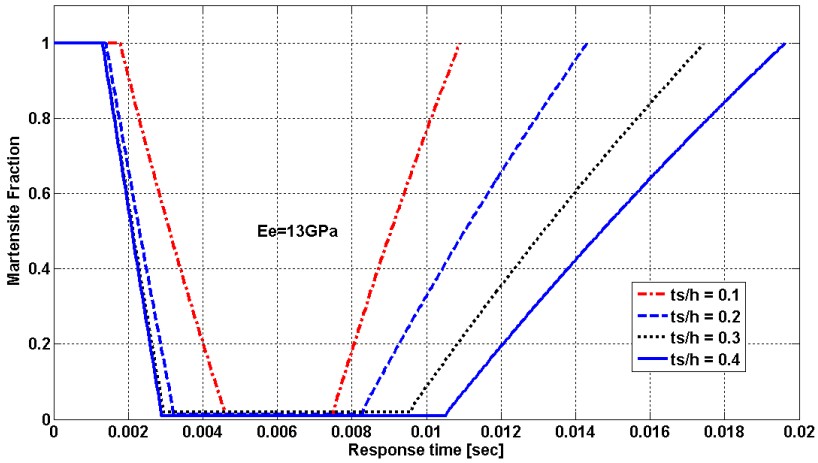


**Figure 16.** SMA thickness effect on the variation of the martensite fraction with time response of the SMA layer in the heating-cooling cycle with input power $P = 2\times10^{7} W/m^{3}$

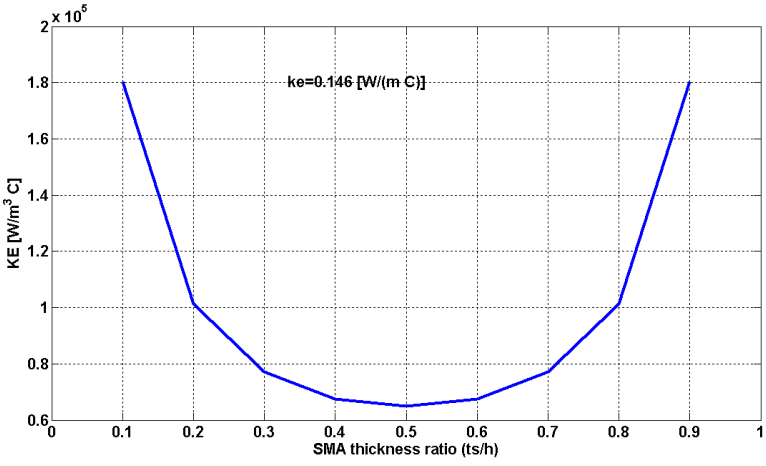


**Figure 17.** SMA thickness ratio (ts/h).

Figures 18 and 19 show the SMA thickness effect on the lateral deflection of SMA laminated cantilever plate before and after activation, respectively. Figures 20 and 21 show SMA thickness effect on the response time and the maximum deflection of SMA laminated cantilever plate at free end with dimensions and dimensionless values, respectively. It is obvious that increasing the SMA layer thickness decreases the plate deflection; this is because of increasing the stiffness of the plate with increasing the SMA thickness ratio. Figure 22 shows the SMA thickness effect on the response time and natural frequency of the proposed cantilever plate. The natural frequency decreases with increasing the SMA thickness ratio, this is because increasing the SMA thickness increases both stiffness and mass of the plate. However, the mass of the plate increases more than its stiffness does, which decrease the natural frequency of the plate.

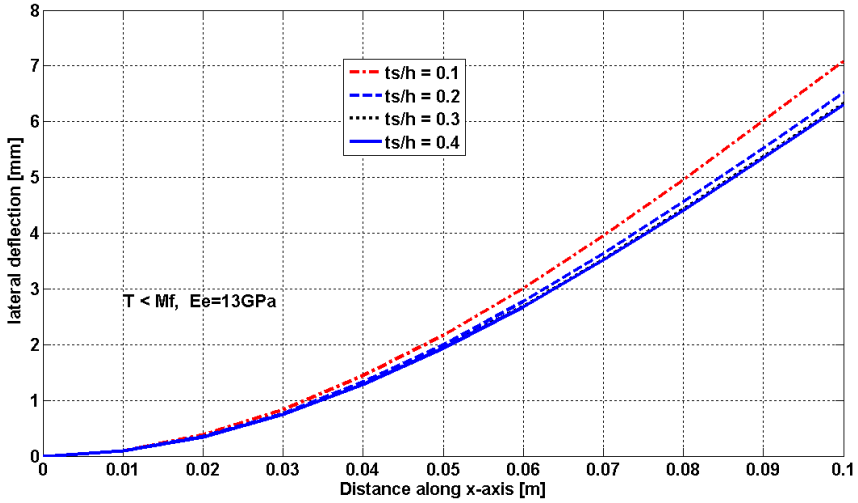


**Figure 18.** SMA thickness effect on the lateral deflection of the plate before activation ($T<M_f$).

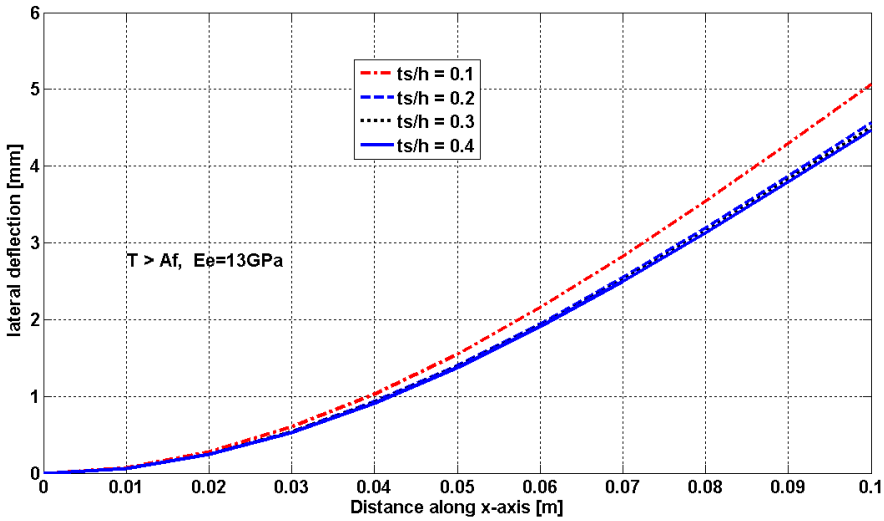


**Figure 19.** SMA thickness effect on the lateral deflection of the plate after activation ($T>A_f$).

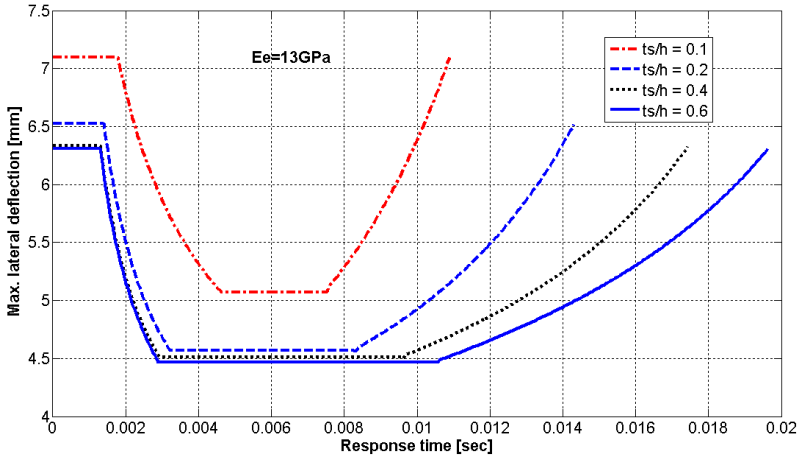


**Figure 20.** SMA thickness effect on the response time and the maximum deflection of the plate at free end (x=a and y=b/2)**.**

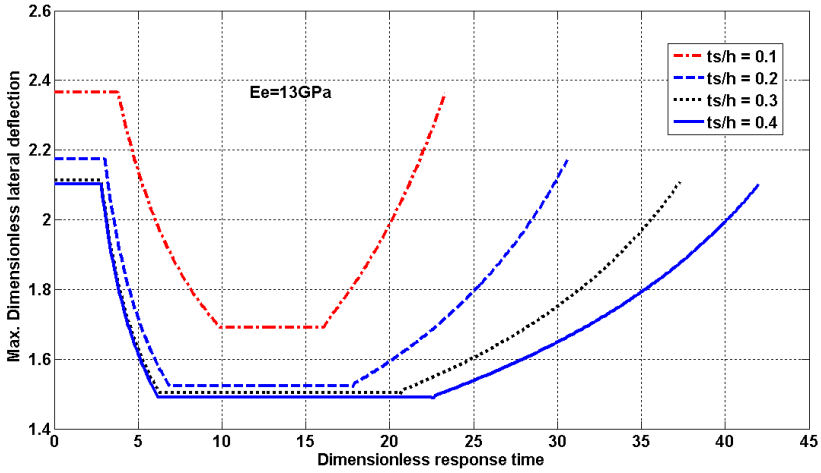


**Figure 21.** SMA thickness effect on both dimensionless response time and the Max. deflection ($\bar{w} = w/h$ ) of the plate at free end (x=a and y=b/2).

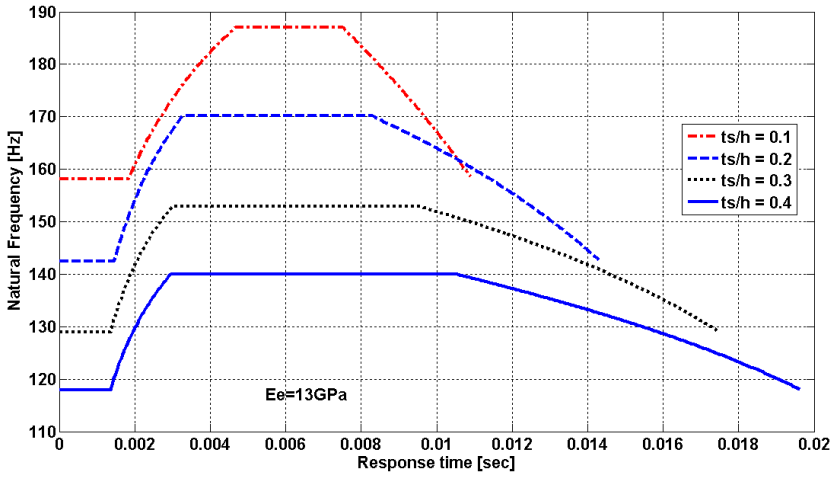


**Figure 22.** SMA thickness effect on the response time and natural frequency of the plate**.**

### (4) Effect of plate aspect and thickness ratios

To study the effect of the plate aspect ratio (a/b) and the thickness ratio (a/h) on the plate deflection and natural frequency, four values of (a/b=1,2,3, and 4) are chosen and a four values of (a/h=10,20,50, and 100) are chosen. The plate length is taken constant (a = 0.1 m) and the SMA thickness ratio is taken constant ($t_s$/h = 0.1) Figure 3. The plate is loaded with a distributed load (q=500 N/m$^2$). The maximum lateral deflection $w\ [mm]$ and its normalized value, $\bar{w}$ , Eq.(44), before and after activation of SMA layer are calculated, and the activation ratios $w$ after activation / $w$ before activation are plotted in Figure 23. The natural frequency, Eq. (44), before and after activation of SMA layer are calculated, and the activation ratios $\omega$ after activation / $\omega$ before activation are plotted in Figure 24. It is clear from Figures 23 and 24.

Figure 23 shows that increasing the plate thickness ratio (a/h) causes decrease of the deflection activation ratio and increase of the natural frequency activation ratio, which means that as the plate becomes thinner; a more response to the SMA activation is obtained. As the plate aspect ratio (a/b) increases, a large response to the SMA activation is obtained.

$$\bar{w} = \frac{10^4 E_e h^3}{a^4 q_0} w\ , \qquad \bar{\omega} = \frac{\omega b^2}{h}\sqrt{\frac{\rho_e}{E_e}} \tag{44}$$

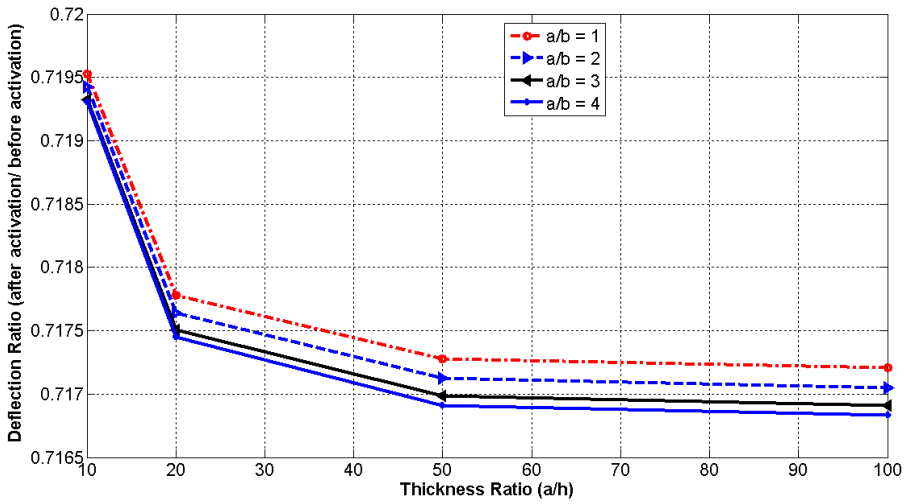


**Figure 23.** The effect of plate thickness ratio (a/h) and aspect ratio (a/b) on the deflection activation ratio $(w\ after\ activation / w\ before\ activation)$ of the plate.

## CONCLUSION

The static response, the dynamic characteristics, and the time response of the shape memory alloy laminated composite plates are obtained and studied. Formulation of static and free vibration problems of laminated composite plates with surface bonded shape memory alloy sheets is presented. Equations of motion with the heat governing equations are deduced based on the modified higher-order shear deformation theory.

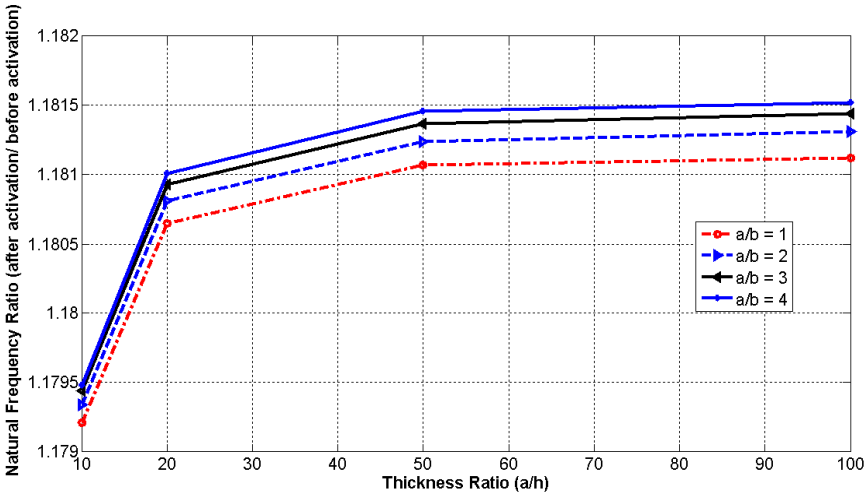


**Figure 24.** The effect of plate thickness ratio (a/h) and aspect ratio (a/b) on the natural frequency activation ratio $(\omega after\ activation / \omega before\ activation)$ of the plate**.**

Parametric studies have been performed and the following conclusions have been drawn:

(1) The lateral deflection of the plate is decreased with the activation of the SMA layer due to the increase of the Young's modulus of the SMA layer in the austenite phase,

(2) Increasing the core material stiffness causes decreasing in deflection without affecting the time response.

(3) Increasing the SMA layer thickness obviously decreases the response time during heating, and increases it during cooling, until the SMA thickness becomes equal to the core thickness $(t_s / h) = 0.5$ then the relation will be inverted.

(4) Increasing the SMA layer thickness decreases both the plate deflection and natural frequency which depends on the ratios of stiffness and mass properties of SMA and core materials.

(5) Increasing the plate thickness ratio (a/h) decreases the deflection activation ratio and increases the natural frequency and activation ratio which means that as the plate becomes thinner, it is more response to the SMA activation.

(6) As the plate aspect ratio (a/b) increases a larger response to the SMA activation is obtained.

(7) The plate deflection is affected by thermal expansion coefficient without affecting the time response, according to the location of the SMA sheet away from the neutral axis and the transverse force direction.

## REFERENCES

[1] M. M. Ghomshei, A. Khajepour, N. Tabandeh and K. Behdinan, "Finite element medeling of shape memory alloy composite actuators: theory and experiment," *Journal of intelligent material systems structures,* vol. 12, pp. 761-773, November 2001.

[2] M. M. Ghomshei, N. Tabandeh, A. Khajepour and K. Behdinan, "Finite element analysis of a new shape memory alloy composite actuator," *http://resonance.uwaterloo.ca/students/mghomshei/ghomshe*, 2000.
[3] B. S. Balapgol, Kamal M. Bajoria and Sudhakar, "A two-dimensional finite element analysis of a shape memory alloy laminated composite plate," *Smart Materials and Structures, 15,* pp. 1009-1020, 2006.
[4] B. S. Balapgol, Kamal M. Bajoria and Sudhakar, "Natural frequencies of mutilayer SMA laminated composte cantilever plate," *Smart Materials and Structures, 15,* pp. 1021-1032, 2006.
[5] F. Gordaninejad and W. Wu, "A two-dimensional shape memory alloy/elastomer actuator," *International Journal of Solids and Structures,* vol. 38, pp. 3393-3409, 2001.
[6] W. Wu, F. Gordaninejad and R. A. Wirtz, "Modeling and analysis of a shape memory alloy- elastomer composite actuator," *Journal of intelligent material systems structures,* vol. 7, pp. 441-447, July 1996.
[7] C. A. Rogers, C. Liang and J. Jia, "Structural modification of simply-supported laminated plates using embedded shape memory alloy fibers," *Computers & Structures,* vol. 38, pp. 569-580, 1991.
[8] M. W. Lin and C. A. Rogers, "Analysis of stress distribution in a shape memory alloy composite beam," *Proceeding of the AIAA/ ASME/ AHS/ ASC 32nd structures, structural dynamics, and material conference , part 1,* vol. AIAA-91-1164-cp, pp. 169-177, 1991.
[9] K. Tanaka, "A phenomenological description on thermomechanical behaviour of SMA," *Journal of Applied Mechanics,* vol. 112, pp. 158-163, 1990.
[10] C. Liang and C. A. Rogers, "One-dimensional thermo-mechanical constitutive relations for shape memory materials," *Journal of intelligent material systems structures* vol. 1, pp. 207-234, 1990.
[11] L. C. Brinson, "One-dimensional constitutive behavior of shape memory alloys: thermomechanical derivation with non-constant material functions and redefined martensite internal variable.," *Journal of intelligent material systems structures,* vol. 4, pp. 229-242, April, 1993.
[12] L. C. Brinson and J. Mater, "Constitutive behaviour of SMA: One-dimensional thermomechanical derivation with non-constant material functions and redefined martensite internal variable," pp. 729-743, 1990.
[13] M. K. Abbas, M. Adnan Elshafei and Hany M. Negm, "Modeling and Analysis of Laminated Composite Plate Using Modified Higher Order Shear Deformation Theory," in *15th International Conference on Aerospace Sciences & Aviation Technology, ASAT-15, May 28- 30*, MTC, Kobry Elkobbah, Cairo, Egypt, 2013, asat@mtc.edu.eg.
[14] M. K. Abbas, "Design and Analysis of Aircraft Composite Structure Using Shape Memory Alloys," Master of Science, Chair of Aircraft Mechanical Engineering, Military Technical College, Cairo, 2013.
[15] J. N. Reddy, *Mechanics of laminated composite plates and shells*, second ed.: CRC Press, 2004.
[16] M. Achenbach and I. Muller, "Simulation of material behaviour of alloys with shape memory," *Arch. Mech.,* vol. 37, No. 6, pp. 573-585, 1985.
[17] R. A. Wirtz, WF Gordaninejad F and W Wu, "Free response of a thermally driven composite actuator," *Journal of intelligent material systems structures,* vol. 6 no.3, pp. 398-406, 1995.

[18] J. N. Reddy, *An Introduction to the Finite Element Method*, Second ed.: McGraw-Hill,Inc, 1993.
[19] D. R. Croft and D. G. Lilley, *Heat transfer calculations using finite difference equations*. London: Applied Science Publishers Ltd., 1977.

## Appendix A

The Evolution equations of Brinson's model

**1- Twinned Martensite → detwinned martensite**
Or (Austenite → detwinned martensite)

a- $T > M_S$ and $\sigma_s^{cr} + C_M (T - M_S) < \sigma < \sigma_f^{cr} + C_M (T - M_S)$

$$\xi_S = \frac{1-\xi_{S0}}{2} \cos\left[ \frac{\pi}{\sigma_s^{cr} - \sigma_f^{cr}} \left( \sigma - \sigma_f^{cr} - C_M \left( T - M_s \right) \right) \right] + \frac{1+\xi_{S0}}{2}$$

$$\xi_T = \xi_{T0} - \frac{\xi_{T0}}{1-\xi_{S0}} \left( \xi_S - \xi_{S0} \right)$$

b- $T < Ms$ and $\sigma_s^{cr} < \sigma < \sigma_f^{cr}$

$$\xi_S = \frac{1-\xi_{S0}}{2} \cos\left[ \frac{\pi}{\sigma_s^{cr} - \sigma_f^{cr}} \left( \sigma - \sigma_f^{cr} \right) \right] + \frac{1+\xi_{S0}}{2}$$

$$\xi_T = \xi_{T0} - \frac{\xi_{T0}}{1-\xi_{S0}} \left( \xi_S - \xi_{S0} \right) + \Delta_{T\xi}$$

If $M_f < T < M_S$ and $T < T_0$

$$\Delta_{T\xi} = \frac{1-\xi_{T0}}{2} \left\{ \cos\left[ a_M \left( T - M_f \right) \right] + 1 \right\}$$

else, $\Delta_{T\xi} = 0$ .9

**2- Martensite → Austenite**

For $T > A_S$ and $C_A (T - A_f) < \sigma < C_A (T - A_S)$

$$\xi = \frac{\xi_0}{2} \left\{ \cos\left[ \frac{\pi}{A_f - A_S} \left( T - A_S - \frac{\sigma}{C_A} \right) \right] + 1 \right\}$$

$$\xi_S = \xi_{S0} - \frac{\xi_{S0}}{\xi_0} \left( \xi_0 - \xi \right)$$

$$\xi_T = \xi_{T0} - \frac{\xi_{T0}}{\xi_0} \left( \xi_0 - \xi \right)$$

**3- Austenite → Twinned Martensite**

For $M_f < T < M_s$, $\sigma < \sigma_s^{cr}$ and $T < T_0$

Putting $\xi_S$ and $\xi_{S0}$ gives the same formula of Liang's model if we put the slope $C_M = \infty$ because the transformation curves at $\sigma < \sigma_s^{cr}$ are vertical lines, [11],

$$\xi = \frac{1-\xi_0}{2}\cos\left[a_M\,(T - M_f)\right] + \frac{1+\xi_0}{2}$$

In this case, the total induced martensite is a pure temperature induced martensite, i.e. $\xi = \xi_T$ and $\xi_0 = \xi_{T0}$.

## Appendix B

Dimensionless parameters of heat equations

| **Dimensionless Parameters** | **Heating** | **Cooling** |
|---|---|---|
| Time, $\tau$ | $t\,k_s/\left(h^2 C_s\right)$ | |
| Temperature, $\theta$ | $(T - A_s)/(A_f - A_s)$ | $(T - M_f)/(M_s - M_f)$ |
| Heat of transition, $R_{MA}$ | $q_s/C_s\,(A_f - A_s)$ | $q_s/C_s\,(M_s - M_f)$ |
| Power ratio, $R_P$ | $Ph^2/k_s\,(A_f - A_s)$ | 0 |
| Heat sink strength, $S$ | $(A_s - T_{\text{sink}})/(A_f - A_s)$ | $(M_f - T_{\text{sink}})/(M_s - M_f)$ |
| Lateral deflection, $\bar{w}$ | $w/h$ | |
| Coordinate, $X$ | $x/h$ | |
| Coordinate, $Y$ | $y/h$ | |
| Conductivity, $R_k$ | $K_E h^2/k_s$ | |